Title
Spin canting of Ni/CoO/Fe films grown on curved MgO(001) substrate

Authors
Yang, M
Li, Q
N'Diaye, AT
et al.

Publication Date
2022-11-01

DOI
10.1016/j.jmmm.2022.169668

Peer reviewed

Spin canting of Ni/CoO/Fe films grown on curved MgO(001) substrate

M. Yang[1,3], Q. Li[2,3,†], A. T. N'Diaye[4], P. Shafer[4], C. Klewe[4], T. Y. Wang[3], Y. Z. Wu[5], Xixiang Zhang[6], C. Hwang[7], and Z. Q. Qiu[3,†]

[1] *Institute of Physical Science and Information Technology, Anhui University, Hefei, Anhui 230601, China*
[2] *National Synchrotron Radiation Laboratory, University of Science and Technology of China, Hefei, Anhui 230029, China*
[3] *Department of Physics, University of California at Berkeley, Berkeley, California 94720, USA*
[4] *Advanced Light Source, Lawrence Berkeley National Laboratory, Berkeley, California 94720, USA*
[5] *Department of Physics and State Key Laboratory of Surface Physics, Fudan University, Shanghai 200433, China*
[6] *Physical Science and Engineering Division (PSE), King Abdullah University of Science and Technology (KAUST), Thuwal 23955-6900, Saudi Arabia*
[7] *Korea Research Institute of Standards and Science, Yuseong, Daejeon 305-340, Korea*

Using element-resolved x-ray magnetic circular dichroism (XMCD) and x-ray magnetic linear dichroism (XMLD) measurements, we determined the spin orientations of Ni, CoO and Fe films in Ni/CoO/Fe films grown on a curved MgO(001) substrate. We find that the vicinal surface of MgO(001) substrate results in a spin canting towards out-of-plane direction in the Ni and CoO films as a result of the interfacial coupling. The Ni spin canting angle increases monotonically with the vicinal angle in the studied range of 0°-17° and the CoO spin canting angle increases more rapidly towards saturation only at a few degrees of the vicinal angle. The uniaxial magnetic anisotropy induced in the Ni layer by the Ni/CoO interfacial coupling is quantitatively determined and is shown to increase monotonically with the vicinal angle. Our result provides a new pathway for tailoring the spin orientation by modifying the substrate surface symmetry in combining with the ferromagnetic/antiferromagnetic interfacial interaction in thin-film based spintronic devices.

PACS numbers: 75.70.Ak

I. INTRODUCTION

Controlling spin orientation in devices is one of the most fundamental topics in spintronic technology such as the magnetic recording, magnetic field sensors, and the nonvolatile memories, etc.[1] In particular, tailoring spin orientation between in-plane and out-of-plane directions has attracted enormous attention because of the importance of perpendicular magnetic anisotropy (PMA) in magnetic materials[2,3]. Among many different methods of modulating the spin orientation of a ferromagnetic (FM) or antiferromagnetic (AFM) thin film, the most common method is to tailor the magnetic anisotropy by growing the FM (AFM) thin film on different substrates. For example, recognizing that magnetocrystalline anisotropy is very sensitive to local crystalline and electronic structures, the common practice of tailoring the magnetic anisotropy is to grow FM (AFM) thin films on substrates with different crystalline orientation[4,5] or with different tensile/compressive strain from lattice mismatching [6,7]. This method is very effective for both conventional FM materials as well as for the recently emerging two-dimensional van der Waals ferromagnet materials[8]. Further extension of this method is growing FM thin films on vicinal surfaces which break in-plane rotational symmetry so that additional in-plane uniaxial magnetic anisotropy can be created in the FM overlayer thin films[9,10,11,12]. Different from the above approach, interfacial coupling between FM and AFM materials is also an effective method to modify the spin orientation of the FM and AFM layers. The advantage of using AFM layer is that FM/AFM interfacial interaction could generate several types of magnetic anisotropies in the FM layer such as the unidirectional anisotropy from the exchange bias[13,14], uniaxial anisotropy from the spin-flop coupling[15,16,17], and the out-of-plane magnetic anisotropy from magnetic frustrations[18,19,20]. From the above discussion, it is interesting to ask whether it is possible to develop a promising method to control the spin orientation of a FM thin film by combining the structural modification of the substrate and the FM/AFM interaction?

In our previous study[21], we found strong evidence that both Ni and CoO spins could cant towards the out-of-plane direction in Ni/CoO/Fe films grown on vicinal MgO(001). The key role played in the whole process is the vicinal surface which is responsible for the CoO spin canting and the Ni uniaxial magnetic anisotropy. Although the underlying mechanism was attributed to the Fe spins which cause a canted CoO spin component that consequently induces the Ni spin canting by the Ni/CoO interfacial coupling, it is unclear on the relation between the vicinal angle and the spin canting angles of the FM and AFM layers. In this paper, we report a comprehensive study of Ni/CoO/Fe sandwich grown on a curved MgO (001) substrate. The use of curved MgO(001) substrate permits a continuous change of the vicinal angle so that films grown on this substrate would have the identical sample growth conditions such as the substrate temperature, film thickness, and oxygen atmosphere, leaving the vicinal angle of the

substrate the only varying parameter. Element-resolved x-ray magnetic circular dichroism (XMCD) and x-ray magnetic linear dichroism (XMLD) measurements were utilized to determine the Ni, CoO and Fe spin orientations separately. We find that the Ni layer shows a spin orientation canting towards the out-of-plane direction, which increases monotonically with the vicinal angle. CoO spin canting angle shows a rapid increase within a few degrees of vicinal angle and saturates at larger vicinal surface. Furthermore, the Ni uniaxial anisotropy induced by the interfacial coupling is also quantitively determined and was shown to increase monotonically with the vicinal angle.

II. EXPERIMENT

MgO/Ni/CoO/Fe/curved MgO(001) multilayer samples were prepared in an ultrahigh vacuum (UHV) system by molecular beam epitaxy (MBE). The MgO(001) substrate was polished into a curved shape with the atomic step edges parallel to the [110] direction [Fig. 1(a)]. The coordinate system was defined as *x*//MgO[110], *y*//MgO[$1\bar{1}0$] and *z*//MgO[001], as shown in Fig. 1(a). The curved substrate serves as multiple local substrates with the vicinal angle α varying continuously from 0° to ~17° [Fig. 1(b)]. The curved substrate was annealed at 600 °C for 10 hours in the UHV chamber, followed by a 5-nm-thick MgO seed layer growing at 500 °C. A 6 nm Fe film was deposited on the substrate at room temperature from an e-beam evaporator. Then a 4 nm CoO film was grown by a reactive deposition of Co under the oxygen pressure of 1.5×10^{-6} Torr[11,21]. A 2.2 nm Ni film was grown on top of the whole substrate with a 2.5 nm MgO capping layer to avoid ambient oxidation. The Fe and CoO epitaxial layers are single crystalline films with the in-plane lattice relation of CoO[110]//Fe[100]//MgO[110] [11,16,17,21] and the Ni film is polycrystalline [see the LEED patterns in Fig. 1 (c)].

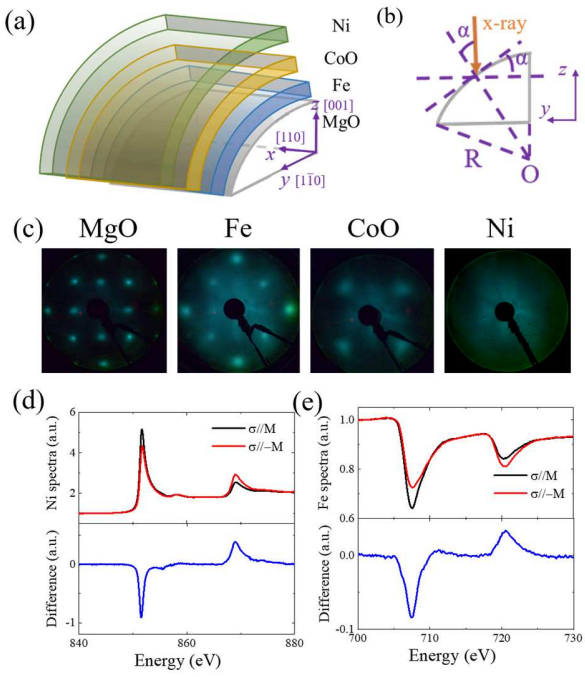

FIG. 1: (a) Schematic drawing of the sample structure on a curved MgO substrate. (b) Schematic drawing of the curved surface in the *yz*-plane. The vicinal angle α is defined as the angle between surface normal direction and the MgO [001] direction (z-axis). The orange arrow represents the incident x-ray beam along -z direction. (c) LEED patterns from sample of MgO(2.5nm)/Ni(2.2 nm)/CoO(4 nm)/Fe(6 nm)/curved MgO(001). (d) Ni x-ray absorption spectra (XAS) and the corresponding XMCD signal. (e) Fe XAS and the corresponding XMCD signal. σ in (d) and (e) represent the incident direction of circular polarized x-ray.

After growth, the sample was brought to Beamline 6.3.1 at the Advanced Light Source (ALS) for XAS, XMCD and XMLD measurements. Since the XMCD measures the projection of the magnetization along the x-ray incident direction and the magnetic field at BL 6.3.1 can be applied only along the x-ray direction, we performed the XMCD measurements for Fe and Ni with the magnetic field parallel and antiparallel to the x-ray incidence direction [Figs. 1 (d), (e)]. The XAS for Ni was collected by total electron yield (TEY) mode, while the XAS for Fe was collected by luminescence yield (LY) mode to overcome the limited probing depth of the TEY mode. The element-resolved XAS and XMCD measurements enable the direct detection of magnetic properties from each of the FM layers in our sample[22,23]. The XMLD measurement of CoO was performed by rotating sample to ensure different incidence angles of linear polarized x-ray. All the measurements were performed at low temperature (~78 K) except mentioned. The sample was cooled down from 330 K with an in-plane magnetic field applied perpendicularly

to the atomic steps [x axis in Fig. 2(a)] of the curved surface. It is known that CoO on vicinal MgO(001) has its in-plane easy magnetization axis parallel to the steps[11] and that the FM/CoO interfacial coupling favors a perpendicular alignment between the Fe and CoO spins due to spin-flop coupling[16,17,24] below CoO's Néel temperature.

III. RESULTS AND DISCUSSION

We first studied the Ni layer magnetic property in Ni/CoO/Fe/curved MgO sample by measuring the Ni hysteresis loops at low temperature. According to our previous result[21], Ni spin is always in the yz-plane, i.e. perpendicular to the atomic steps (x axis) below the CoO's Néel temperature (T_N). Therefore, we focused our discussion on the Ni spin direction in the yz-plane in this work. Firstly, the hysteresis loops were taken for x-ray beam along the -z direction [Fig. 2(a), θ=0°] with the magnetic field sweeping along the x-ray incidence direction. The hard-axis loop with nearly zero remanence shows that the easy axis (EA) of Ni magnetization is fully in the film plane at near zero vicinal angle of α=0.8° [Fig. 2(c)]. Then we studied the Ni remanence at θ=0° as a function of the vicinal angle α by measuring the Ni hysteresis loops at different positions [along y direction in Fig. 2(a)] of the curved MgO substrate. Fig. 2(d) and (e) show two selected Ni hysteresis loops at vicinal angles of 6.5° and 17.3°, respectively. The hysteresis loops clearly show a non-zero remanence, indicating that the Ni easy magnetization axis cants towards the out-of-plane direction, i.e. there is an obvious z-component of the Ni magnetization at zero magnetic field. Then we performed the Ni hysteresis loop measurement at three represented locations of the curved substrate (labeled as the black square, blue triangle and red circle at Fig. 2(a)) with vicinal angles of α=0.8°, 6.5° and 17.3° and at various incidence angles of the x-rays. The relative magnetic remanence (M_r/M_S) was extracted from each hysteresis loop and plotted in Fig. 2(b) as a function of the x-ray incidence angle θ. The magnetic remanence shows a symmetric behavior around θ=0° at α=0.8°, indicating the absence of Ni spin canting (i.e. Ni spin is fully in-plane which is consistent with the result in Fig. 2(c)). However, the magnetic remanence at vicinal angles of α=6.5° and 17.3° shows a symmetric center away from θ=0°, indicating that the Ni spin cants towards out-of-plane direction. Since XMCD measures the projection of the magnetization to the x-ray direction, the Ni magnetization EA direction can be determined quantitatively using the following formula:

$$M_r/M_S = |\cos(\theta\text{-}\theta_{Ni})|. \qquad (1)$$

Here θ_{Ni} is defined as the angle between the Ni EA direction and MgO[001] direction [z direction in Fig. 2(a)]. Then $\theta_{Ni} - \alpha$ is the angle of Ni EA away from the vicinal surface normal direction [Fig. 2(i)], i.e., $\phi_{Ni} \equiv 90° - (\theta_{Ni} - \alpha)$is the Ni spin canting angle towards the out-of-plane direction [Fig. 2(i)]. By fitting the θ-dependent remanence signal, we obtained θ_{Ni}=90° for vicinal angle α=0.8° (i.e., the Ni EA is in plane, Fig. 2(h))), and θ_{Ni}=76° for α=6.5° (i.e., the Ni EA cants 20.5° out of the vicinal surface) and θ_{Ni}=70° for α=17.3° (i.e., the Ni EA cants 37.3° out of the vicinal surface, Fig. 2(i)).

To obtain the relationship between the Ni spin canting angle and the substrate vicinal angle, the Ni magnetic hysteresis loops at various vicinal angles were taken at three x-ray incident angles of θ=-30°, 0°, 30°. The remanence of the Ni hysteresis loops at θ=30° and θ=-30° overlaps at M_r/M_S=0.5 for vicinal angle of 0°, which is consistent with the projection of in-plane magnetization at vicinal angle of 0° along x-ray incidence direction [Fig. 2(f)]. With increasing the vicinal angle, the difference between the magnetic remanence at θ=-30° and θ=30° increases monotonically [Fig. 2(g)]. By fitting the remanence result using Eqn. (1), we obtained the Ni EA direction as a function of the vicinal angle. We summarized the Ni spin canting angle (ϕ_{Ni}) as a function of the vicinal angle in Fig. 2(g). The result shows that the Ni spin canting angle increases monotonically with the vicinal angle and reaches about 37.3° at vicinal angle α=17.3°.

Our previous study demonstrated that an in-plane Fe magnetization in Ni/CoO/Fe/vicinal MgO(001) leads to a spin canting of CoO due to Fe/CoO interfacial coupling. To verify the generality of this result for all vicinal angles, we performed the XMCD/XMLD measurement to determine the Fe and CoO spin cantings on the curved substrate. We first took the Fe magnetic hysteresis loops with circular polarized x-rays at three selected spots [Fig. 3(a)]. Fig. 3(b) shows the represented Fe hysteresis loops at incident angles of θ=-30°, 30° at the blue triangle position (α=6.5°). The almost identical magnetic hysteresis loops for these two cases indicate the absence of Fe spin canting at this vicinal angle. Then we performed the hysteresis loop measurement at different x-ray incident angles at three vicinal angles and extracted the Fe magnetic remanence as a function of θ [Fig. 3(c)]. The Fe remanence in all three cases is symmetric to 0°, indicating an in-plane Fe spin orientation throughout the curved films. Quantitative fittings using $M_r/M_S = |\cos(\theta\text{-}\theta_{Fe})|$ further confirmed this conclusion (i.e., θ_{Fe}=90°).

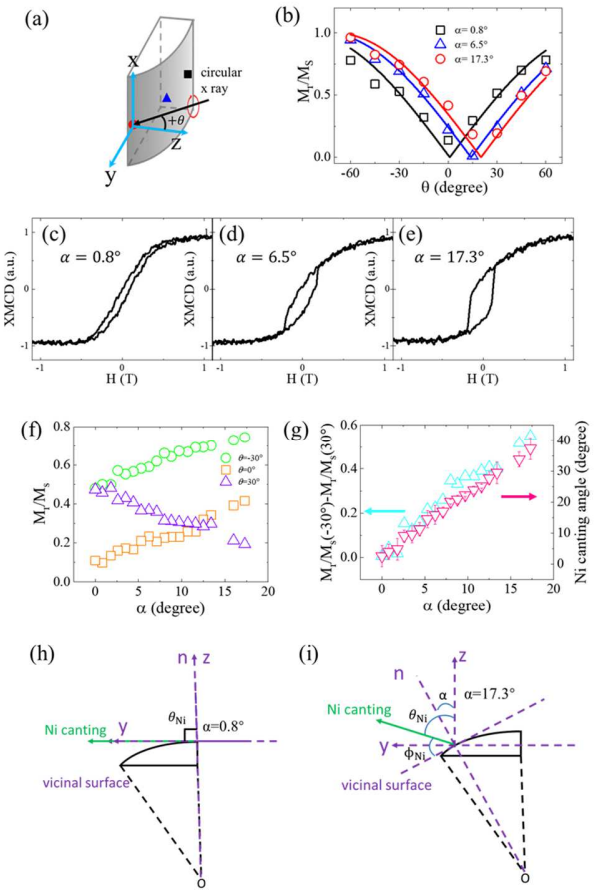

FIG. 2: (a) Schematic drawing of measurement configuration for Ni XMCD hysteresis loops at three selected vicinal angles. The black square, blue triangle and red circle represent the measure positions for vicinal angles of 0.8°, 6.5° and 17.3°, respectively. (b) Ni magnetic remanence as a function of θ at the three selected vicinal angles. Ni XMCD hysteresis loops for (c) α=0.8°, (d) α=6.5° and (e) α=17.3° with normal incident circular x-rays. (f) Ni remanence as a function of vicinal angle α with circular x-ray incidence angles of -30°, 0° and 30°. (g) The difference of Ni magnetic remanence at θ=30° and θ=-30° and the Ni canting angle as a function of α. Schematic drawing of Ni EA, the angle of α, θ_{Ni} and ϕ_{Ni} in *yz*-plane at vicinal angles of (h) α =0.8° and (i) α=17.3°.

As reported in our previous studies, CoO spin axis is mainly parallel to the atomic steps (x direction) but with a small canting component in the *yz*-plane[21]. To determine the AFM CoO spin canting direction in the *yz*-plane, we took Co L_3 edge absorption spectra (XAS) using linearly polarized x-rays (Fig. 3(a)). Fig. 3(d) shows the representative Co L_3 edge XAS with linearly polarized x-rays at +30° and -30° incident angles for vicinal angle of 6.5° at 78 K. There is an obvious difference at the peaks of ~777 eV, 778.3 eV, 778.8 eV and 779.6 eV at the two incidence angles of linear polarized x-ray, indicating the existence of the x-ray linear dichroism (XLD). To avoid the complexity effect of charge anisotropy in the XLD[25], we define the CoO R_{L3} ratio as the intensity ratio of peaks at ~778.3 eV over the peak at ~778.8 eV as denoted by the two arrows in Fig. 3(d). The θ-dependent CoO R_{L3} ratio at the three selected measurement locations are shown in Fig. 3(e). Both the crystal-field effect and the AFM order contribute to the XLD at the Co L_3 edge[11,21]. While the AFM contribution vanishes above Néel temperature, the crystal-field effect persists at high temperature[26,27]. Thus the R_{L3} ratio curve at 330 K is due to the crystal-field effect and the three R_{L3} ratio curves at 78 K come from both the crystal-field effect and the AFM order contribution. All these R_{L3} (θ) curves show a clear quadratic dependence on the sinusoidal θ, and indeed can be well fitted by $R_{L3}(\theta)=A\cos^2(\theta-\theta_{CoO})+B$[10,28]. To single out the magnetic contribution to R_{L3}, we defined $\Delta R_{L3} \equiv R_{L3}(78K)-R_{L3}(350K)$ to eliminate the crystal-field effect. From fittings of $\Delta R_{L3}(\theta)$ in Fig. 3(f), we obtained θ_{CoO} = 4.8°, 40.2°, 50.8° from sample at vicinal angles of α=0.8°,6.5°,17.3°, respectively. This result unambiguously demonstrates that the CoO spin canting angle towards the out-of-plane direction increases at larger vicinal angles. Moreover, the increase of amplitude from fittings of $\Delta R_{L3}(\theta)$ in Fig. 3(f) suggests the increasing component of the CoO spin in the *yz*-plane at larger vicinal angle.

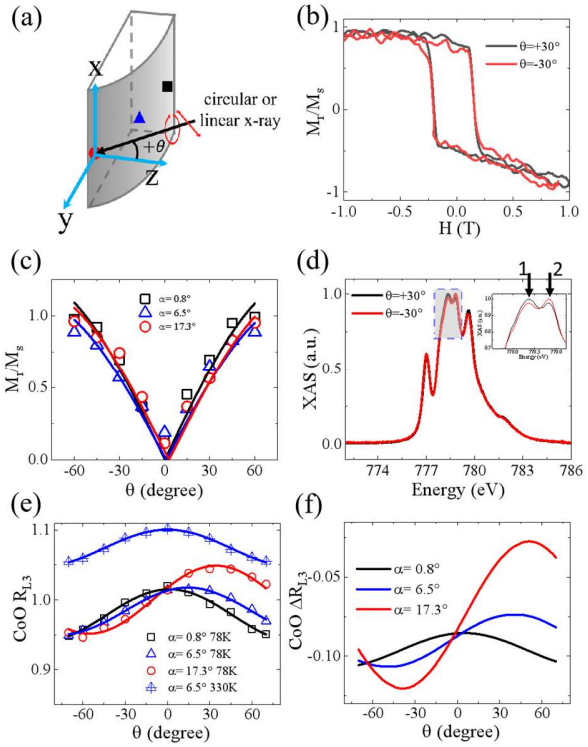

FIG. 3: Schematic drawing of measurement configurations for (a) Fe XMCD hysteresis loops and (d) CoO XAS at three selected vicinal angles. The black square, blue triangle and red circle represent the measure positions

for vicinal angles of α=0.8°, 6.5° and 17.3°, respectively. (b) Fe magnetic hysteresis loops with circularly polarized x-rays at θ=+30° and -30° incident angles for vicinal angle of α=6.5°. (c) Fe magnetic remanence as a function of θ at three selected vicinal angles. The solid lines are the fittings of Fe remanence using Eqn. (1). (d) Co L_3 edge absorption spectra with linearly polarized x ray at +30° and -30° incidence angles for vicinal angle of 6.5°. Inset is the enlarged spectra of the dashed area which shows the peaks at ~778.3 eV and ~778.8 eV. (e) CoO R_{L3} ratio as a function of incidence angle θ for three selected vicinal angles at 78 K and for 6.5° at 330 K. Solid lines are fittings using $R_{L3}(\theta)=A\cos^2(\theta-\theta_{CoO})+B$. (f) Lines of CoO $\Delta R_{L3}(\theta)$ from subtraction of fitting lines in (e) as a function of incidence angle θ.

To further confirm the relationship between the CoO spin canting angle and the vicinal surface angle, we carried out the XAS measurements with x-rays at incident angles of θ=-60°, -30°, 0°, 30° and 60° at different vicinal angles α. Then after fitting the R_{L3} ratios using $\Delta R_{L3}(\theta)=A\cos^2(\theta-\theta_{CoO})+B$, we obtained the CoO spin canting angle ϕ_{CoO}, which is defined as the angle of CoO EA relative to the vicinal sample surface, i.e. $\theta_{CoO}-\alpha$ in Fig. 4(a), as a function of vicinal angle α [Fig. 4(b)]. To compare the Ni spin canting angle and CoO spin canting angle, we also plotted the Ni spin canting angle (e.g. ϕ_{Ni} in Fig. 4(a)) in Fig. 4(b)). We found that Ni spin canting angle increases monotonically with the vicinal angle while the CoO spin canting angle shows a rapid increase within a few degrees of vicinal angle and then saturates at larger vicinal angle.

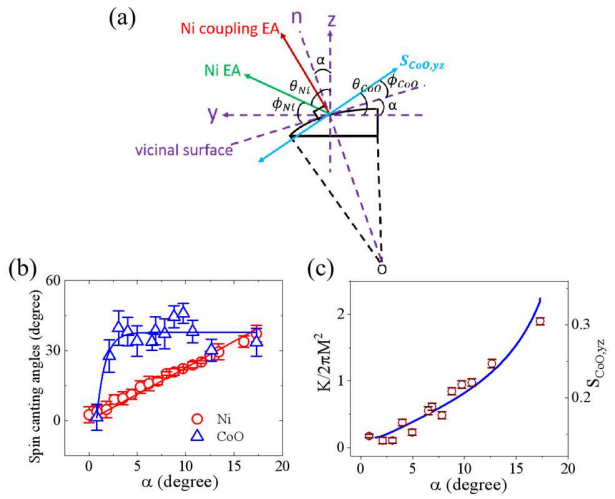

FIG. 4: (a) Schematic drawing of Ni and CoO spin orientation on curved MgO(001) surface in *yz*-plane. Ni EA denotes the easy axis of Ni layer, and Ni coupling EA denotes the CoO/Ni exchange coupling-induced EA in Ni layer, which is perpendicular to the *yz* component of CoO spin ($S_{CoO,yz}$). (b) Ni canting angles and CoO canting angles as a function of vicinal angle α. The solid lines are guide to the eye. (c) Open symbols represent the *yz* component of CoO spin as a function of vicinal angle α. Solid line is a guide to the eye about the uniaxial anisotropy $K/2\pi M^2$ as a function of the vicinal angle α.

Since we found that the CoO/Fe magnetic interfacial coupling on a vicinal surface could modify the CoO spin configuration and consequently induce a uniaxial magnetic anisotropy in the Ni film, it is natural to consider the competition between the Ni/CoO interfacial coupling energy and the demagnetization energy of the Ni layer in the remanence state when analyzing the Ni spin canting on curved substrate[21]. For the spin configuration shown in Fig. 4(a), the Ni energy density is given by

$$E = 2\pi M^2 \sin^2\phi_{Ni} - K\sin^2(\phi_{Ni}+\phi_{CoO}) \quad (3)$$

Here M is the Ni saturation magnetization, K is the uniaxial anisotropy constant induced by the magnetic coupling between Ni and the *yz* component of the CoO spins in the *yz*-plane, ϕ_{CoO} is the CoO spin angle which can be obtained from the fitting of $\Delta R_{L3}(\theta)$ curve. The Ni uniaxial anisotropy $K/2\pi M^2$ can be obtained by minimizing the energy density with respect to the Ni magnetization angle $\frac{\partial E}{\partial \phi_{Ni}}=0$:

$$K/2\pi M^2 = \frac{\sin(2\phi_{Ni})}{\sin(2\phi_{Ni})\cos(2\phi_{CoO})+\sin(2\phi_{CoO})\cos(2\phi_{Ni})} \quad (4)$$

Using this formular, we calculated Ni uniaxial anisotropy as a function of vicinal angle α [Fig. 4(c)] based on the Ni and CoO spin canting angles in Fig. 4(b). The initial increase of Ni uniaxial anisotropy at a few degrees of vicinal angle could be attributed to the rapid increase of CoO spin canting angle. Fig. 4(c) shows the summarized CoO *yz* component, which was obtained through fitting of CoO $\Delta R_{L3}(\theta)$ with the relation of $S_{CoO,yz}$ being proportional to the squareroot of XMLD amplitude as shown in Fig. 3(f). We found $S_{CoO,yz}$ as a function of vicinal angle shows similar trend with the curve of the Ni uniaxial anisotropy, showing that the Ni uniaxial anisotropy is induced by CoO spin cantings in the *yz*-plane.

IV. SUMMARY

In summary, we studied Ni and CoO spin cantings in Ni/CoO/Fe/curved MgO(001) sample. By determining the Ni spin orientation through XMCD hysteresis loop measurement and the CoO Néel vector orientation through XMLD analysis, we show that both Ni and CoO spins cant towards out-of-plane direction with increasing the vicinal angle. Furthermore, the Ni uniaxial anisotropy induced by the interfacial coupling between Ni and CoO spin cantings in the *yz*-plane is also quantitively determined to monotonically increase with the vicinal angle. Our result on

the continuous spin canting orientation provides a new route to control the spin orientation in magnetic thin films.

ACKNOWLEDGMENTS

The authors would like to express their deepest gratitude to Prof. Chia-Ling Chien, a pioneer in the field of magnetism, who inspired generations of scientists and educators worldwide. This work was supported by US Department of Energy, Office of Science, Office of Basic Energy Sciences, Materials Sciences and Engineering Division under Contract No. DE-AC02-05-CH11231 (van der Waals heterostructures program, KCWF16). This research used resources of the Advanced Light Source, which is a DOE Office of Science User Facility under contract no. DE-AC02-05CH11231 and and Beamlines MCD-A and MCD-B (Soochow Beamline for Energy Materials) at NSRL. This work was supported by National Natural Science Foundation of China (Grant No. 12174364, 12104003, 11734006 and 11974079), Users with Excellence Program of Hefei Science Center CAS (No. 2021HSC-UE003), Fundamental Research Funds for the Central Universities (No. wk2310000104), Natural Science Foundation of Anhui Province (Grant No. 2108085QA20), Open Fund of State Key Laboratory of Surface Physics of Fudan University (No. KF2020_06, KF2021_05), Future Materials Discovery Program through the National Research Foundation of Korea (No. 2015M3D1A1070467), Science Research Center Program through the National Research Foundation of Korea (No. 2015R1A5A1009962) and King Abdullah University of Science and Technology (KAUST) under Award No. ORA-CRG10-2021-4665. The nanofabrication in this work was carried out at the USTC Center for Micro and Nanoscale Research and Fabrication.

†Email addresses: liqian89@ustc.edu.cn; qiu@berkeley.edu

References:

[1] J. Nogués, I. K. Schuller, J. Magn. Magn. Mater. **192**, 203 (1999).

[2] F. Hellman, A. Hoffmann, Y. Tserkovnyak, G. S. D. Beach, E. E. Fullerton, C. Leighton, A. H. MacDonald, D. C. Ralph, D. A. Arena et al., Rev. Mod. Phys. **89**, 025006 (2017).

[3] A. Fert, N. Reyren, and V. Cros, Nat. Rev. Mater. **2**, 17031 (2017).

[4] J. Nogues, T. J. Moran, D. Lederman, I. K. Schuller, and K. V. Rao, Phys. Rev. B **59**, 6984 (1999).

[5] E. Młyńczak, B. Matlak, A. Kozioł-Rachwał, J. Gurgul, N. Spiridis, and J. Korecki, Phys. Rev. B **88**, 085442 (2013).

[6] S. I. Csiszar, M. W. Haverkort, Z. Hu, A. Tanaka, H. H. Hsieh, H.-J. Lin, C. T. Chen, T. Hibma, and L. H. Tjeng, Phys. Rev. Lett. **95**, 187205 (2005).

[7] Z. Chen, Z. Chen, C.-Y. Kuo, Y. Tang, L. R. Dedon, Q. Li, L. Zhang, C. Klewe, Y.-L. Huang, B. Prasad, A. Farhan, M. Yang, J. D. Clarkson, S. Das, S. Manipatruni, A. Tanaka, P. Shafer, E. Arenholz, A. Scholl, Y.-H. Chu, Z.Q. Qiu, Z. Hu, L.-H. Tjeng, R. Ramesh, L.-W. Wang and L. W. Martin, Nat. Commun. **9**, 3764 (2018).

[8] L. Zhang, L. Song, H. Dai, J.-H. Yuan, M. Wang, X. Huang, L. Qiao, H. Cheng, X. Wang, W. Ren, X. Miao, L. Ye, K.-H. Xue, and J.-B. Han, Appl. Phys. Lett. **116**, 042402 (2020).

[9] Y. Z. Wu, C. Won, and Z. Q. Qiu, Phys. Rev. B 65, 184419 (2002).

[10] Y. Z. Wu, Z. Q. Qiu, Y. Zhao, A. T. Young, E. Arenholz and B. Sinkovic, Phys. Rev. B **74**, 212402 (2006).

[11] Q. Li, T. Gu, J. Zhu, Z. Ding, J. X. Li, J. H. Liang, Y. M. Luo, Z. Hu, C. Y. Hua, H.-J. Lin, T. W. Pi, C. Won and Y. Z. Wu, Phys. Rev. B **91**, 104424 (2015).

[12] Q. Li, M. Yang, A. T. N'Diaye, C. Klewe, P. Shafer, N. Gao, T. Y. Wang, E. Arenholz, Xixiang Zhang, C. Hwang, J. Li and Z. Q. Qiu, Phys. Rev. Mater. **3**, 114415 (2019).

[13] M. Kiwi, J. Magn. Magn. Mater. 234, 584 (2001).

[14] M. Grimsditch, A. Hoffman, P. Vavassori, H. T. Shi and D. Lederman, Phys. Rev. Lett. **90**, 257201 (2003).

[15] T. C. Schulthess and W. H. Butler, Phys. Rev. Lett. **81**, 4516 (1998).

[16] Q. Li, G. Chen, T. P. Ma, J. Zhu, A. T. N'Diaye, L. Sun, T. Gu, Y. Huo, J. H. Liang, R. W. Li, C. Won, H. F. Ding, Z. Q. Qiu and Y. Z. Wu, Phys. Rev. B **91**, 134428 (2015).

[17] M. Yang, Q. Li, D. Hou, P. Shafer, A. T. N'Diaye, C. Klewe, T. Y. Wang, Xixiang Zhang, C. Hwang and Z. Q. Qiu, Phys. Rev. B **101**, 224418 (2020).

[18] B.-Y. Wang, J.-Y. Hong, K.-H. O. Yang, Y.-L. Chan, D.-H. Wei, H.-J. Lin and M.-T. Lin, Phys. Rev. Lett. **110**, 117203 (2013).

[19] J. Wu, J. Choi, A. Scholl, A. Doran, E. Arenholz, C. Hwang and Z. Q. Qiu, Phys. Rev. B **79**, 212411 (2009).

[20] P. Kuswik, P. L. Gastelois, M. M. Soares, H. C. N. Tolentino, M. De Santis, A. Y. Ramos, A. D. Lamirand, M. Przybylski, and J. Kirschner, Phys. Rev. B **91**, 134413 (2015).

[21] Q. Li, M. Yang, A. T. N'Diaye, Q. Y. Dong, A. Scholl, A. T. Young, N. Gao, E. Arenholz, C. Hwang, J. Li, and Z. Q. Qiu, Phys. Rev. B **96**, 214405 (2017).

[22] Q. Li, M. Yang, C. Klewe, P. Shafer , A.T. N'Diaye, D. Hou, T. Y. Wang, N. Gao, E. Saitoh, C. Hwang, R. J. Hicken, J. Li, E. Arenholz and Z. Q. Qiu, Nat. Commun. **10**, 5265 (2019).

[23] A. D. Bang, I. Hallsteinsen, F. K. Olsen, S. D. Sloetjes, S. T. Retterer, A. Scholl, E. Arenholz, E. Folven, and J. K. Grepstad, Appl. Phys. Lett. **114**, 192403 (2019).

[24] J. Wu, J. S. Park, W. Kim, E. Arenholz, M. Liberati, A. Scholl, Y. Z. Wu, Chanyong Hwang, and Z. Q. Qiu, Phys. Rev. Lett. **104**, 217204 (2010).

[25] G. van der Laan, E. Arenholz, R. V. Chopdekar, and Y. Suzuki, Phys. Rev. B **77**, 064407 (2008).

[26] D. Alders, L. H. Tjeng, F. C. Voogt, T. Hibma, G. A. Sawatzky, C. T. Chen, J. Vogel, M. Sacchi, and S. Iacobucci, Phys. Rev. B **57**, 11623 (1998).

[27] M. W. Haverkort, S. I. Csiszar, Z. Hu, S. Altieri, A. Tanaka, H. H. Hsieh, H.-J. Lin, C. T. Chen, T. Hibma, and L. H. Tjeng, Phys. Rev. B **69**, 020408(R) (2004).

[28] W. Kim, E. Jin, J. Wu, J. Park, E. Arenholz, A. Scholl, C. Hwang, and Z. Q. Qiu, Phys. Rev. B **81**, 174416 (2010).